Electrical and optical properties of $C_{46}H_{22}N_8O_4KM$ (M=Co, Fe, Pb) molecular-material thin films prepared by the vacuum thermal evaporation technique

M.E. Sánchez-Vergara [a,*], M.A. Ruiz Farfán [a], J.R. Álvarez [b], A. Ponce Pedraza [a], A. Ortiz [c], C. Álvarez Toledano [d]

[a] *Mechanical Engineer Department, Instituto Tecnológico y de Estudios Superiores de Monterrey, Campus Ciudad de México, Calle del Puente 222, Col. Ejidos de Huipulco, 14380, México, DF, México*
[b] *Electric and Electronic Engineer Department, Instituto Tecnológico y de Estudios Superiores de Monterrey, Campus Ciudad de México, Calle del Puente 222, Col. Ejidos de Huipulco, 14380, México, DF, México*
[c] *Instituto de Investigaciones en Materiales. Universidad Nacional Autónoma de México, A P 70-360, Coyoacán, 04510, México, DF, México*
[d] *Inorganic Chemistry Department, Instituto de Química, Universidad Nacional Autónoma de México, Circuito Exterior, Ciudad Universitaria, 04510, México, DF, México*

Abstract

In this work, the synthesis of new materials formed from metallic phthalocyanines (Pcs) and double potassium salt from 1,8-dihydroxianthraquinone is reported. The newly synthesized materials were characterized by scanning electron microscope (SEM), atomic force microscopy (AFM), infrared (IR) and Ultraviolet–visible (UV–vis) spectroscopy. The powder and thin-film samples of the synthesized materials, deposited by vacuum thermal evaporation, show the same intra-molecular bonds as in the IR spectroscopy studies, which suggests that the thermal evaporation process does not alter these bonds. The effect of temperature on conductivity and electrical conduction mechanism was measured in the thin films ($\sim$137 nm thickness). They showed a semiconductor-like behaviour with an optical activation energy arising from indirect transitions of 2.15, 2.13 and 3.6 eV for the $C_{46}H_{22}N_8O_4KFe$, $C_{46}H_{22}N_8O_4KPb$ and $C_{46}H_{22}N_8O_4KCo$ thin films.
© 2006 Elsevier B.V. All rights reserved.

Keywords: Organic semiconductors; Electrical properties and measurements; Anisotropy

1. Introduction

Phthalocynanines (Pcs) have been extensively studied for their applications in nonlinear optics and electronic device materials [1–3]. Phtalocyanines are regarded as good candidates for nonlinear optical applications [4]. On the other hand, Pcs have excellent electrical properties, including the ability to form resilient, semi-conducting thin films and the capacity to undergo molecular and structural modifications in order to control some of their properties [5].

Electrical conductivity of Pcs can be directly evaluated on thin films when the interaction between the substrate and the molecular thin film is weak enough to prevent dissociative chemical absorption [6]. Pcs have macrocyclic 18-π-electron systems which enable them to form very stable organic photo-semiconductors (OPCs) [5]. In addition to their excellent photoconductive properties, Pcs are very stable against thermal and chemical decomposition [4]. They may also be employed as active materials in molecular electronic devices such as displays, chemical sensors [7] and optical data storage components [8]. A great effort has recently been made to study the optical properties of Pcs and related compounds. Due to the high optical absorption of these molecules in the UV–vis region, there is a considerable interest in the characterization of the electronic structure of Pcs [4]. Since most Pcs exhibit particularly high optical absorption and emission in the 550–700 nm range of the spectrum, they can be considered as good candidates for optical applications in this range [4].

The aim of this paper is to report the synthesis and characterization of three new semi-conducting materials based on lead,

---

* Corresponding author. Tel.: +52 55 5483 2199; fax: +52 55 5483 2163.
  E-mail address: sanchez.mariaelena@gmail.com (M.E. Sánchez-Vergara).

cobalt and iron Pcs with a double potassium salt derived from 1,8-dihydroxiantraquinone. The refractive indices and absorption coefficients have been determined for the studied samples. Both parameters, refractive indices and absorption coefficients, are of particular interest in metal-organic semiconductors for the design and fabrication of optoelectronic devices, such as laser heterostructures [9]. Thermal evaporation and ellipsometry have been employed in the growth and characterization of the new thin films, as ellipsometry is a very sensitive characterization technique that has proved its usefulness in the study of surface roughness and interlayer formation in multilayer thin-film systems [9]. The optical band gap and some electrical properties of the resulting thin films have been measured, including the electrical conductivity and electronic band gap.

2. Experimental procedure

The chemicals for this work were obtained from commercial sources with no purification prior to their use. Carbon, hydrogen and nitrogen elementary analysis were performed at the Chemical Coordination Laboratory in Toulouse (France). Vibrational spectra were acquired with a Perkin-Elmer IR spectrophotometer model 282-B using KBr pellets.

Synthesis of $C_{46}H_{22}N_8O_4KFe$: dissolve 0.18 g (0.57 mmol) of double potassium salt from 1,8-dihydroxianthraquinone in 20 ml of methanol for an hour. Then add 0.17 g (0.28 mmol) of iron phtalocyanine chloride and keep it in reflux for 72 h. Cool at room temperature, filter and wash with methanol. The resulting brown powder was dried under high vacuum, yielding 92% of the reaction. Calculated analysis for $C_{46}H_{22}N_8O_4KFe$: C, 65.32; H, 2.6; and N, 13.25. Found: C, 65.19; H, 2.37; and N, 13.19. IR (KBr, cm^{-1}) ν_{max}: 1622(C–H); 1494(C–C); and 1119(C=N).

Synthesis of $C_{46}H_{22}N_8O_4KPb$: add 0.14 g (0.19 mmol) of lead phtalocyanine to 0.28 g (0.89 mmol) of double potassium salt from 1,8-dihydroxianthraquinone and dissolve it in 20 ml of methanol. Reflux for 72 h. Cool at room temperature, filter and wash with methanol. The resulting magenta powder was dried under high vacuum, yielding 89% of the reaction. Calculated analysis for $C_{46}H_{22}N_8O_4KPb$: C, 61.6; H, 2.46, and N, 12.5. Found: C, 61.96; H, 2.41; and N, 12.0. IR (KBr, cm^{-1}) ν_{max}: 1615(C–H); 1508(C–C); and 1114(C=N).

Synthesis of $C_{46}H_{22}N_8O_4KCo$: add 0.11 g (0.19 mmol) of cobalt phtalocyanine to 0.22 g (0.7 mmol) of double potassium salt from 1,8-dihydroxianthraquinone and dissolve it in 20 ml of methanol. Reflux for 72 h. Cool at room temperature, filter and wash with methanol. The resulting purple powder was dried under high vacuum, yielding 87% of the reaction. Calculated analysis for $C_{46}H_{22}N_8O_4KCo$: C, 65.09; H, 2.59; and N, 13.2. Found: C, 65.94; H, 2.25; and N, 13.37. IR (KBr, cm^{-1}) ν_{max}: 1615(C–H); 1508(C–C); and 1123(C=N).
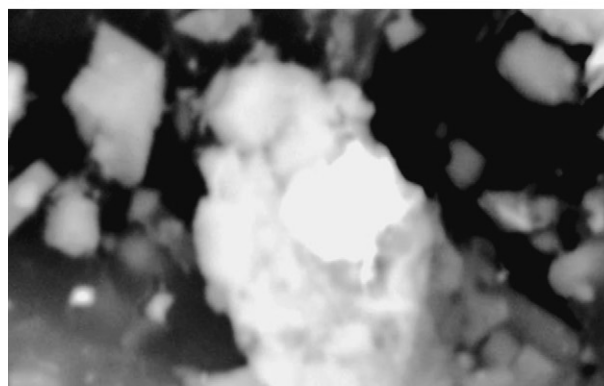
2.1. Thin films

Corning 7059 glass, a vacuum thermal vaporizer with diffusion pump and C–Si substrates were used for thin-film preparation. Scanning electron microscopy (SEM) was carried out in a Leica Cambridge, Stereoscan 440 model with a coupled micro-

analysis system including X-ray energy dispersive spectrometer (EDS). A focal distance of 25 mm and a 20-kV potential were used for all samples. An atomic force microscope (AFM) coupled to a potentiostat/galvanostat module from Digital Instruments (NanoScope IIIA) was also used to investigate the morphology of the complexes. Fourier transform infrared spectroscopy (FTIR) measurements for thin films were made with a Nicolet 5-MX spectrophotometer. Ellipsometric measurements were made with a Gaertner ellipsometer (model L117), using a He–Ne laser operating at a wavelength of 630 nm. UV–vis transmittance measurements were made with a Shimadzu 260
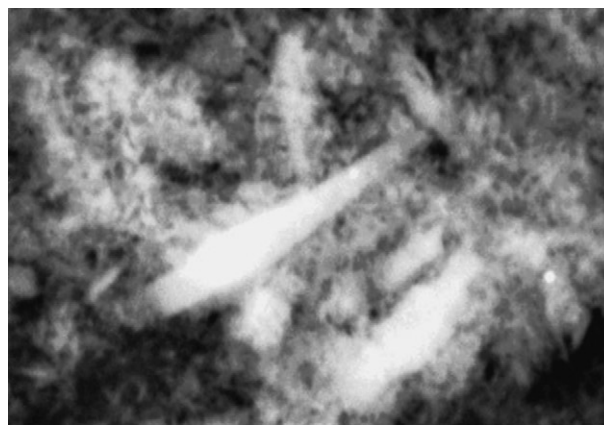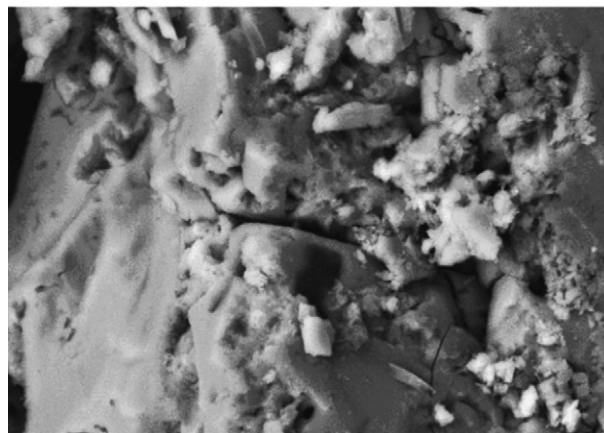
Fig. 1. SEM micrograph of material: (a) $C_{46}H_{22}N_8O_4KFe$ at 5000×; (b) $C_{46}H_{22}N_8O_4KPb$ at 8500×; and (c) $C_{46}H_{22}N_8O_4KCo$ at 1000×.

double-beam spectrophotometer. To measure the temperature dependence of thin-film current, a Keithley 230 V source and a Keithley 485 picoammeter, coupled to a PC-controlled HP3421 data acquisition system, were used.

Thin-film deposition was carried out by vacuum thermal evaporation onto 7059 Corning glass slices and monocrystalline silicon wafers, ultrasonically degreased in warm ethanol and dried in a nitrogen atmosphere. To prevent the powder products from reaching the surface of the substrate, a molybdenum boat with two grids was used as the evaporation source. The boat temperature was 473 °C during evaporation, as measured with a chromel–alumel thermocouple. It must be noticed that the synthesized compound sublimates. For infrared and ellipsometric measurements, the substrates were oriented along the (1 0 0) direction. Each substrate was made of 200 Ω cm CSi. For the optical transmission measurements, the substrates were bare 7059 Corning glass slices. The electrical conductivity of the films was studied by means of a four-probe using 7059 Corning glass substrates coated with four metallic strips. These metallic strips acted as electrodes for the electrical measurements. In order to get an ohmic behaviour between the deposited films and the metallic electrodes, four gold or silver strips were deposited by vacuum thermal evaporation onto the glass slices.

3. Results and discussion

The SEM micrographs of the $C_{46}H_{22}N_8O_4KFe$, $C_{46}H_{22}N_8O_4KPb$ and $C_{46}H_{22}N_8O_4KCo$ compounds are shown in Fig. 1. In all cases, the thin films showed a granular appearance. The surface of the deposited films was composed of elon-
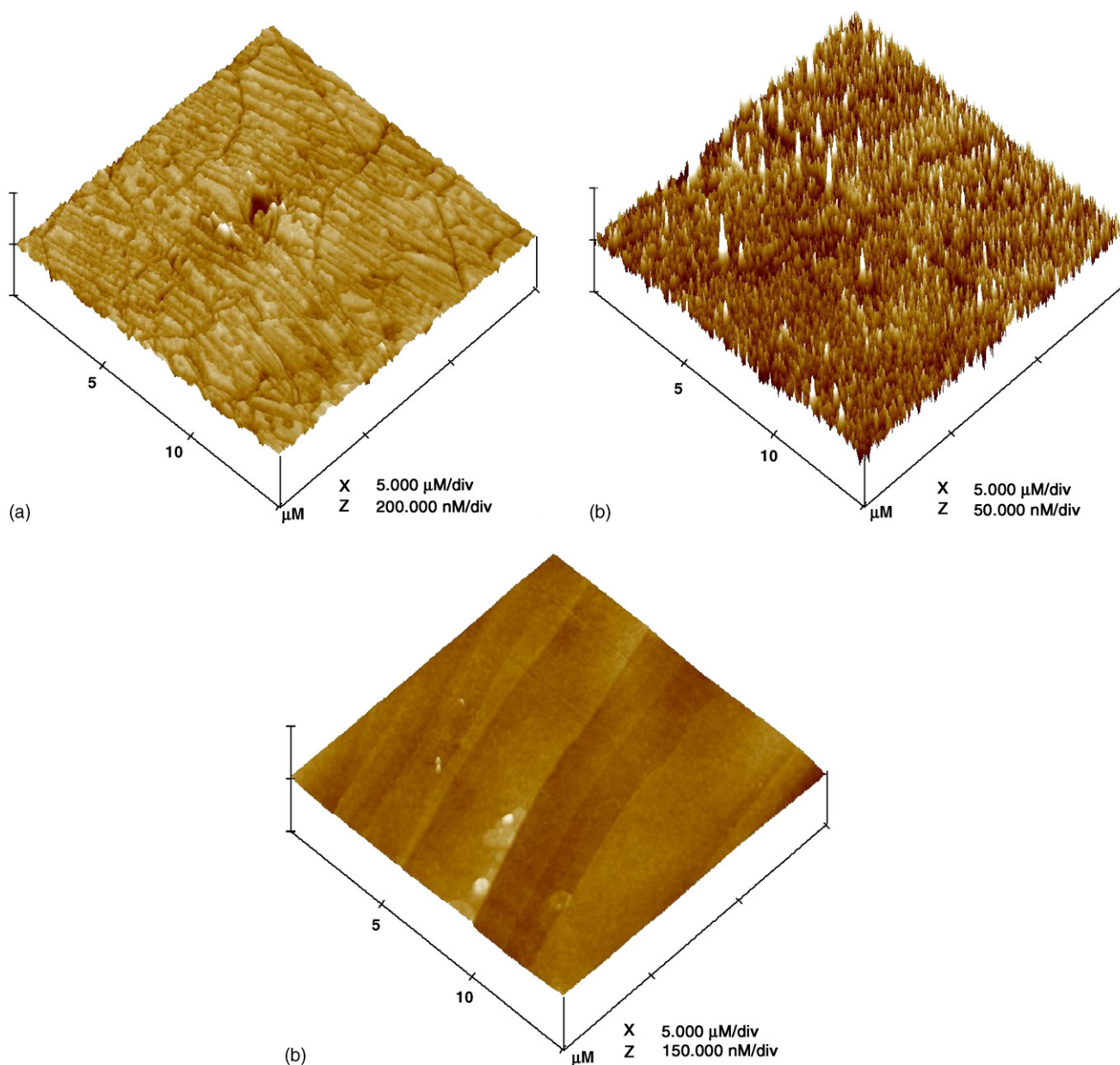

Fig. 2. Three-dimensional AFM images of: (a) $C_{46}H_{22}N_8O_4KFe$; (b) $C_{46}H_{22}N_8O_4KPb$; and (c) $C_{46}H_{22}N_8O_4Kco$.

Table 1
IR (cm^{-1}) characteristic bands for thin films

Compound	ν(C—H) (cm^{-1})	ν(C—C) (cm^{-1})	ν(C=N) (cm^{-1})
C$_{46}$H$_{22}$N$_8$O$_4$KFe	1620	1496	1117
C$_{46}$H$_{22}$N$_8$O$_4$KPb	1616	1510	1112
C$_{46}$H$_{22}$N$_8$O$_4$KCo	1617	1507	1125

gated and small structures in C$_{46}$H$_{22}$N$_8$O$_4$KFe and granules in C$_{46}$H$_{22}$N$_8$O$_4$KPb and C$_{46}$H$_{22}$N$_8$O$_4$KCo.

AFM was used independently to assess the surface quality of the new materials. Fig. 2 shows 3D AFM images of C$_{46}$H$_{22}$N$_8$O$_4$KFe, C$_{46}$H$_{22}$N$_8$O$_4$KPb and C$_{46}$H$_{22}$N$_8$O$_4$KCo thin films. As the images show, the C$_{46}$H$_{22}$N$_8$O$_4$KFe complex produced some clear modifications on the surface. Although the surface is flat, its texture is irregular with several lines crossing the surface. On the other hand, the C$_{46}$H$_{22}$N$_8$O$_4$KPb film presents a fine granular texture while C$_{46}$H$_{22}$N$_8$O$_4$KCo shows some spots on the surface.

IR spectroscopy was used to determine the presence of the most important and representative functional groups and if there were significant chemical changes in the materials during the thermal evaporation process. Since the thermal stability of these compounds is quite high, no chemical changes or reactions are expected to occur. Table 1 shows the characteristic bands for these compounds' films. These results suggest that film formation is not affected by the thermal evaporation and deposition processes. The deposited films are formed by the same macroions as those of the original synthesized compounds, given that the locations of the absorption bands in the spectra of the synthesized powders and the deposited films are nearly the same. It is worth noting that a slight difference is always expected in all thin films deposited by any method since the inner stresses in the films affect the angles and energies of the intra-molecular bonds.

The UV–vis optical transmission spectra were analyzed in the strong absorption edge region. Pcs present two typical absorption bands, namel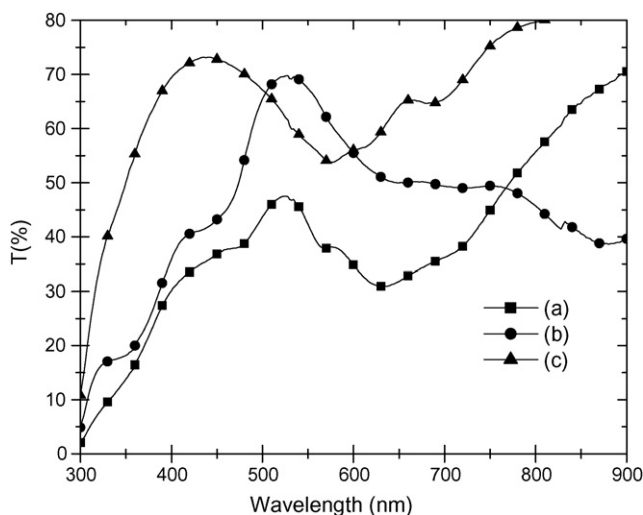y the Q band in the visible region (550–800 nm) and the B or Soret band in the near ultraviolet region (300–400 nm) [10]. The UV–vis spectra for each synthesized material is shown in Fig. 3, including the Q and B bands attributed to π–π^* transitions in the macrocycle of the phthalocyanines. For C$_{46}$H$_{22}$N$_8$O$_4$KFe, the B band is present at 300 nm and the Q band is located at 620 nm, whereas the B and Q bands for the C$_{46}$H$_{22}$N$_8$O$_4$KPb compound are located at 360 and 620 nm, respectively. The corresponding locations for the B and Q bands in C$_{46}$H$_{22}$N$_8$O$_4$KCo are 300 and 560 nm, respectively. The maximum absorption peak in the Q band is assigned to the wavelength remote region because of the presence of the double potassium salt from 1,8-dihydroxianthraquinone. Since the bidentate ligand may increase the interface distance between macrocycles, the direct π–π orbital overlap is not produced and the Q band remains unchanged. The presence of the absorption band may be interpreted as an overlap of π orbitals through the ligand. On the other hand, the different metallic ions in the macrocycle generate differences in the wavelength values assigned to the bands. According to Kumar et al. [2], the incorporation of metallic ions in the Pc molecule may affect the intensity and spacing of the band, but it does not significantly change the general structure of the molecule.

The width of the optical band gap (E_g) can be approximated from a straight-line fit in the $(\alpha h\nu)^{1/2}$ versus $(h\nu)$ plot. The absorption coefficient α near the band edge in many amorphous semiconductors shows a potential dependence on photon energy usually obeying Urbach's empirical relation [11]:

$$\alpha h\nu = \beta(h\nu - E_g)^n \qquad (1)$$

where β^{-1} is the band edge parameter, n is a number characterizing the transition process which takes values 1/2, 1, 2 or 3/2, depending on the nature of the electronic transitions responsible for the absorption [12]. In amorphous semiconductors, the optical transitions are dominated, to a first approximation, by the so-called non-direct transitions. In these electronic transitions, from states in the valence band to states in the conduction band, there is no conservation of the electronic momentum [13].
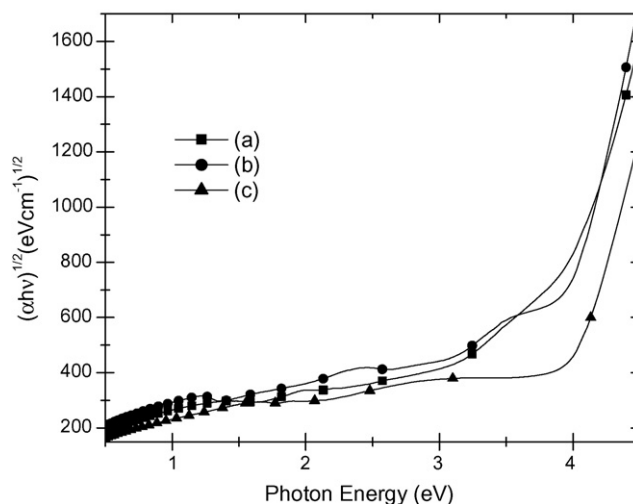

Fig. 3. UV–vis spectroscopy of: (a) C$_{46}$H$_{22}$N$_8$O$_4$KFe; (b) C$_{46}$H$_{22}$N$_8$O$_4$KPb; and (c) C$_{46}$H$_{22}$N$_8$O$_4$KCo.

Fig. 4. Dependence of $(\alpha h\nu)^{1/2}$ as function of the photon energy $h\nu$ for thin films of: (a) C$_{46}$H$_{22}$N$_8$O$_4$KFe; (b) C$_{46}$H$_{22}$N$_8$O$_4$KPb; and (c) C$_{46}$H$_{22}$N$_8$O$_4$KCo.
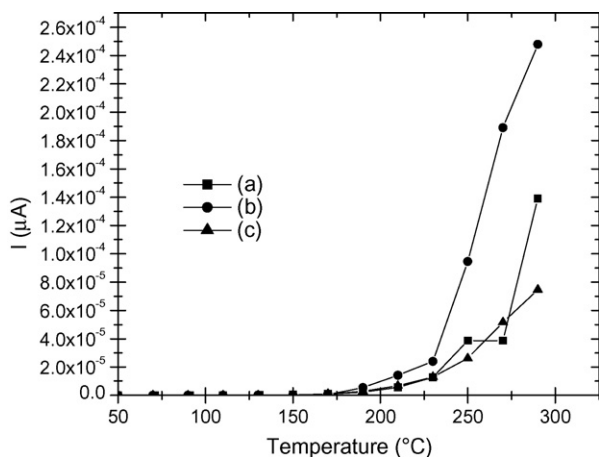
Fig. 5. Electric current variation with temperature for: (a) $C_{46}H_{22}N_8O_4KFe$; (b) $C_{46}H_{22}N_8O_4KPb$; and (c) $C_{46}H_{22}N_8O_4KCo$.

Fig. 4 shows the $(\alpha h\nu)^{1/2}$ versus $(h\nu)$ plot for the thin films. The band gap values of $C_{46}H_{22}N_8O_4KFe$, $C_{46}H_{22}N_8O_4KPb$ and $C_{46}H_{22}N_8O_4KCo$ thin films were found to be 2.15, 2.13 and 3.6 eV, respectively.

The variation of the electrical current with temperature on thin films was evaluated by using the four-probe method. Fig. 5 shows the electric current dependence on temperature at a constant applied voltage in the ohmic regime for each compound's thin film. The curves for the three molecular materials suggest a semiconductor-like behaviour. The lead compound shows a much higher electrical current at 200 °C and above.

The electrical conductivity and its dependence on temperature were investigated in order to distinguish metallic from semiconductor-like behaviours. Fig. 6 shows the semiconductor behaviour of the three synthesized materials. It can be noticed that conductivity increases with temperature for all of them.
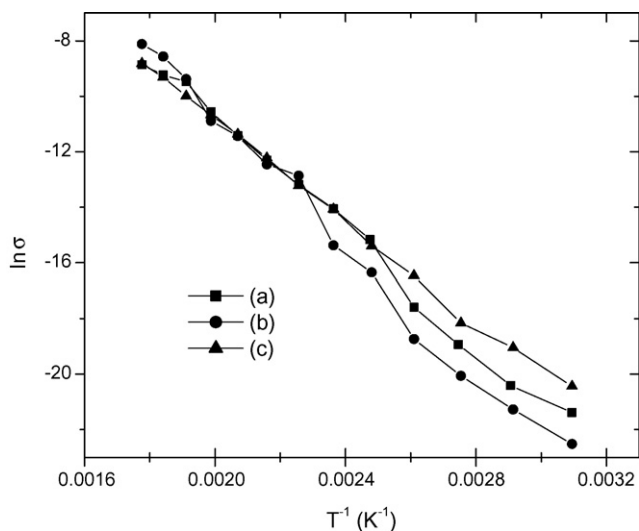

Fig. 6. Electrical conductivity as a function of temperature of: (a) $C_{46}H_{22}N_8O_4KFe$; (b) $C_{46}H_{22}N_8O_4KPb$; and (c) $C_{46}H_{22}N_8O_4KCo$ in thin films deposited on glass.

From the above results, the electrical conductivity of all materials was evaluated at 25 °C and is shown in Fig. 6. The conductivity values found for $C_{46}H_{22}N_8O_4KFe$, $C_{46}H_{22}N_8O_4KPb$ and $C_{46}H_{22}N_8O_4KCo$ are 1.69×10^{-5}, 1.57×10^{-5} and $1.12 \times 10^{-5} \, \Omega^{-1} \, cm^{-1}$, respectively. The iron-based material presents a higher electrical conductivity than the other ones. The conductivity values of all materials at room temperature are very similar and lie in the semiconductor region (10^{-6} to $10 \, \Omega^{-1} \, cm^{-1}$) [14,15]. This is remarkable since a molecular semiconductor is generally defined in terms of its room-temperature conductivity besides its temperature dependence.
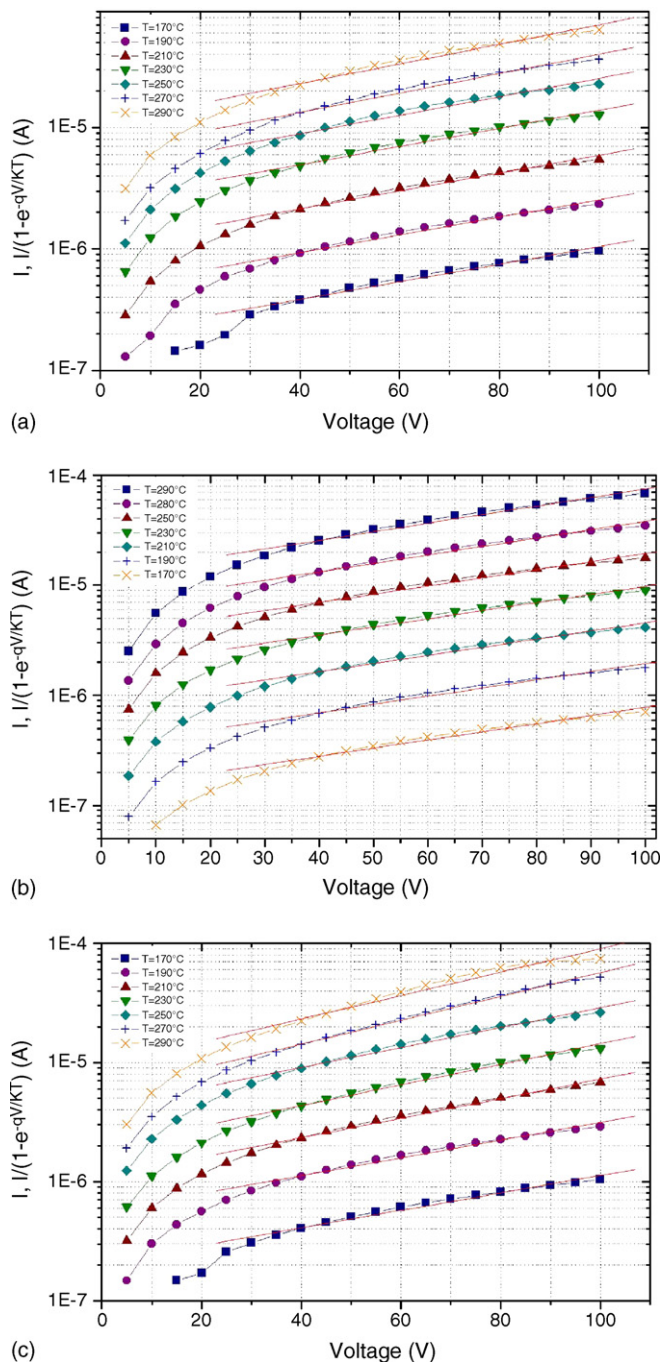

Fig. 7. Log(I) vs. V for samples: (a) $C_{46}H_{22}N_8O_4KFe$; (b) $C_{46}H_{22}N_8O_4KPb$; and (c) $C_{46}H_{22}N_8O_4KCo$.

The specific conductivity σ of Pc films depends on the absolute temperature T as described by the equation

$$\sigma = \sigma_0 \exp\left(-\frac{E_a}{kT}\right) \qquad (2)$$

where σ_0 is the pre-exponential factor, E_a is an activation energy for electrical conductivity and k is Boltzmann's constant [16]. Calculated values of E_a are 1.77, 1.77 and 1.58 eV for $C_{46}H_{22}N_8O_4KFe$, $C_{46}H_{22}N_8O_4KPb$ and $C_{46}H_{22}N_8O_4KCo$, respectively. These E_a values are lower than the result obtained for the optical band gap, which suggests that E_a is an activation energy involving both the energy necessary to excite electrons from the localized states toward extended states through the mobility edge, and the electrical conduction by means of the hopping mechanism between localized states.

In order to determine the electrical conduction mechanism in the thin films, current–voltage (I–V) measurements were carried out at different temperatures. The temperature range considered varies from 170 to 290 °C. Typical Schottky forward biased I–V graphs are observed for the samples. In this way, $\log(I)$ versus V data are plotted for the samples. A thermionic current–voltage behaviour is observed for each curve. The relevant equation [17] was

$$I = I_s \exp\left(\frac{qV}{nkT}\right)\left[1 - \exp\left(\frac{-qV}{kT}\right)\right] \qquad (3)$$

where k is Boltzmann's constant, q is the electrical charge, and n is a factor of ideality; this factor incorporates all those effects making the device nonideal. Data plotted according to Eq. (3) as $\log(I)$ versus V are linear only for $V \gg kT$ as shown in Fig. 7.

In the current–voltage methods, the barrier height is most commonly calculated from the current I_s, determined by extrapolating the $\log(I)$ versus V curve to $V = 0$, i.e., the current-axis intercept for the straight-line portion of the semi-log plot at $V = 0$ is given by I_s. Current–temperature graphs permit us then to study the size of the barrier as a function of temperature. Fig. 8 shows a plot of $\log(I_s/T^2)$ versus $1/T$ for the samples, where I_s values were obtained from the intercept of $\log(I)$ versus V plots
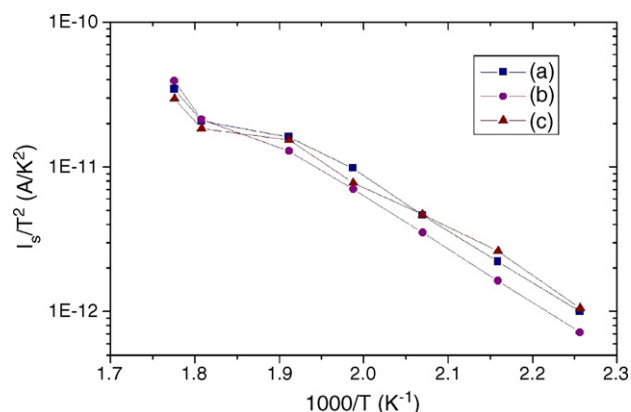
at each temperature. We may observe that the $\log(I_s/T^2)$ versus $1/T$ graphs strongly suggest a behaviour similar to that expected from a thermionic emission current. I–V results are in agreement with those results showing an increase in conductivity with temperature.

4. Conclusions

New semiconductor materials from iron, lead and cobalt phthalocyanines and double potassium salt derived from 1,8-dihydroxianthraquinone were synthesized. Thin films of these materials were deposited by vacuum thermal evaporation. They were formed by the same chemical units as those of the corresponding synthesized powders. The thermal evaporation process did not change intra-molecular bonding, suggesting that the deposition process can be considered as a molecular process.

The optical transitions were found to be of a non-direct nature. The band gap measured in the $C_{46}H_{22}N_8O_4KCo$ thin film was remarkably larger than the gaps measured in the $C_{46}H_{22}N_8O_4KFe$ and $C_{46}H_{22}N_8O_4KPb$ thin films. From the optical band-gap values, the magnitude of the electrical conductivities and the feasibility of preparing these compounds in thin films, these materials may have a potential use in electronic device fabrication.

Concerning to the electrical conduction in the thin films, a thermionic emission is observed as a function of temperature of current–voltage measurements. Data plotted are linear only for $V \gg kT$ range. In this way, current of saturation-temperature plots ($\log(I_s/T^2)$ versus $1/T$) have been carried out, which suggest a behaviour similar to that expected from a thermionic emission current. Electrical conduction mechanism results are in agreement with those results showing an increase in conductivity with temperature.

Acknowledgment

References

[1] D. Scgekettwein, M. Kaneko, A. Yamada, D. Wöhrle, N.I. Jaeger, J. Phys. Chem. 95 (1991) 1748.
[2] G.A. Kumar, G. Jose, V. Thomas, N.V. Unnikrishnan, V.P.N. Nampoori, Spectrochim. Acta (2003) 1.
[3] H.S. Nalwa, J.S. Shirk, in: C.C. Leznoff, A.B.P. Lever (Eds.), Phthalocyanines: Properties and Applications, vol. 4, VCH, New York, 1996.
[4] E.J. Osburn, L.-K. Chau, S.-Y. Chen, N. Collins, D.F. O'Brien, N.R. Armstrong, Langmuir 12 (1996) 4784.
[5] K. Soo-Jong, M. Michiko, S. Kiyotaka, J. Porphyrins Phthalocyanines 4 (2000) 136.
[6] N.R. Armstrong, J. Porphyrins Phthalocyanines 4 (2000) 414.
[7] R.A. Collins, K.A. Mohammed, J. Phys. D21 (1988) 154.
[8] D. Gu, Q. Chen, J. Shu, X. Tang, G. Fuxi, S.K. Sten, X. Xu, Thin Solid Films 88 (1995) 257.
[9] M. Sridharan, Sa. K. Narayandass, D. Mangalaraj, J. Mater. Sci.: Mater. Electr. 13 (2002) 471.
[10] K. Tokumaru, J. Porphyrins Phthalocyanines 5 (2001) 77.

Fig. 8. $\log(I/T^2)$ vs. $(1/T)$ for samples: (a) $C_{46}H_{22}N_8O_4KFe$; (b) $C_{46}H_{22}N_8O_4KPb$; and (c) $C_{46}H_{22}N_8O_4KCo$.

[11] F. Urbach, Phys. Rev. 92 (1953) 1434.

[12] S. Adachi, Optical Properties of Crystalline and Amorphous Semiconductors, Kluwer Academic Publishers, Boston, 1999.

[13] G.D. Cody, in: J.I. Pankove (Ed.), Hydrogenated Amorphous Silicon, Part B, Optical Properties, Semiconductors and Semimetals, vol. 21, Academic Press, Orlando, 1984.

[14] J. Simon, F. Tournillac, New J. Chem. 11 (1997) 383.

[15] J. Simon, New J. Chem. 10 (1986) 295.

[16] A.E. Pochtenny, A.V. Misevich, Tech. Phys. Lett. 1 (2003) 56.

[17] S.M. Sze, Physics of Semiconductor Devices, Wiley-Interscience, New York, 1981.